

## Accepted Manuscript

Tube-based robust model predictive control for spacecraft proximity operations in the presence of persistent disturbance

M. Mammarella, E. Capello, H. Park, G. Guglieri, M. Romano

PII: S1270-9638(17)32122-3  
DOI: <https://doi.org/10.1016/j.ast.2018.04.009>  
Reference: AESCTE 4514

To appear in: *Aerospace Science and Technology*

Received date: 17 November 2017  
Revised date: 9 March 2018  
Accepted date: 5 April 2018

Please cite this article in press as: M. Mammarella et al., Tube-based robust model predictive control for spacecraft proximity operations in the presence of persistent disturbance, *Aerosp. Sci. Technol.* (2018), <https://doi.org/10.1016/j.ast.2018.04.009>

This is a PDF file of an unedited manuscript that has been accepted for publication. As a service to our customers we are providing this early version of the manuscript. The manuscript will undergo copyediting, typesetting, and review of the resulting proof before it is published in its final form. Please note that during the production process errors may be discovered which could affect the content, and all legal disclaimers that apply to the journal pertain.



# Tube-based Robust Model Predictive Control for Spacecraft Proximity Operations in the Presence of Persistent Disturbance

M. Mammarella<sup>a,\*</sup>, E. Capello<sup>b</sup>, H. Park<sup>c</sup>, G. Guglieri<sup>a</sup>, M. Romano<sup>c</sup>

<sup>a</sup>Department of Mechanical and Aerospace Engineering, Politecnico di Torino, Corso Duca degli Abruzzi 24, 10129, Torino, Italy

<sup>b</sup>Department of Mechanical and Aerospace Engineering, CNR-IEIT, Politecnico di Torino, Corso Duca degli Abruzzi 24, 10129, Torino, Italy

<sup>c</sup>Department of Mechanical and Aerospace Engineering, Naval Postgraduate School, 1 University Circle, Monterey, CA 93943, USA

---

## Abstract

Rendezvous and Proximity Operations (RPOs) of two autonomous spacecraft have been extensively studied in the past years, taking into account both the strict requirements in terms of spacecraft dynamics variations and the limitations due to the actuation system. In this paper, two different Model Predictive Control (MPC) schemes have been considered to control the spacecraft during the final phase of the rendezvous maneuver in order to ensure mission constraints satisfaction for any modeled disturbance affecting the system. Classical MPC suitably balances stability and computational effort required for online implementation whereas Tube-based Robust MPC represents an appealing strategy to handle disturbances while ensuring robustness. For the robust scheme, the computational effort reduction is ensured adopting a time-varying control law where the feedback gain matrix is evaluated offline, applying a Linear Matrix Inequality approach to the state feedback stabilization criterion. An extensive verification campaign for the performance evaluation and comparison in terms of constraint satisfaction, fuel consumption and computational cost, i.e. CPU time, has been carried out on both a three degrees-of-freedom (DoF) orbital simulator and an experimental testbed composed by two Floating Spacecraft Simulators reproducing a quasi-frictionless motion. Main conclusions are drawn with respect to the mission expectations.

*Keywords:* Robust Control, Model Predictive Control, Automated Rendezvous and Docking

---

## 1. Introduction

Automated rendezvous and docking (RVD) missions have been widely studied in the last ten years. During these missions, controlled trajectories, in which a Chaser spacecraft tries to reach and dock a Target spacecraft, are guaranteed by a control system, able to handle uncertainties and external environment disturbances. Different control techniques have been proposed in literature, including feedback-linearization-based approach [1], Riccati equation techniques [2], sliding-mode control (SMC) [3], and other control setups in [4, 5]. In [1] the problem of motion synchronization of free-flying robotic spacecraft and serviceable floating objects in space is considered, but a limitation of this approach is that the linear system can be different from the nonlinear one, due to the cancellation of nonlinearities. The Riccati equation techniques (as in [2]) are simple, numerically stable and competitive in computational effort with other known methods. However, only small parametric uncertainties are included. In [3] SMC strategies are proposed for thruster control, even if it is deemed to lead to excessive fuel consumption, due to switching on/off thrusters at high frequency. Even if a fuel-efficient algorithm is proposed, a high consumption is verified to track the docking port. As clearly explained in [4], a model predictive control approach for spacecraft proximity maneuvering which could effectively handle the constraints on thrust magnitude, line-of-sight, and approach velocity, and can

be more effective than other controllers in terms of fuel consumption.

For this reason, in this research, special attention has been reserved to the adoption of MPC, for its ability to deal with the constraints that typically characterize this maneuver, both in terms of relative position and velocity, as well as actuation system limitations. The approach proposed here moves along the lines of previous works employing MPC schemes for RVD. A Linear Quadratic MPC (LQMPC) has been adopted to enforce thrust magnitude limitation, line of sight (LOS) constraints, and velocity constraints for soft docking in [6]. In [7], a low-complexity MPC scheme for three degree-of-freedom (DoF) spacecraft system is developed for the low-thrust rendezvous and proximity operations.

However, in all of these approaches, orbital perturbations, disturbances, and model errors are not taken into account. In [8], the improved performance of a robust MPC in the presence of disturbances, compared with a classical one, are highlighted solving the spacecraft rendezvous problem. In the last years, focusing on robust approach, a new appealing approach has been introduced, called Tube-based Robust MPC (TRMPC), which focuses on two main goals: (i) the robustness to additive disturbances and (ii) the computational efficiency of a classical MPC. Moreover, this algorithm is split in two parts: (i) an offline evaluation of the constraints to ensure the uncertain future trajectories lie in sequence of sets, known as *tubes*, and (ii) the online MPC scheme applied to the nominal trajectories, representing the center of the tube itself as in [9].

The main ideas of this paper are to evaluate the perfor-

---

\*corresponding author

Email address: [martina.mammarella@polito.it](mailto:martina.mammarella@polito.it) (M. Mammarella)

mance of a robust MPC controller, both in simulations and on an experimental setup, and to demonstrate the real-time effectiveness of the proposed robust approach. Moreover, this proposed MPC controller is able to handle uncertainties due to external disturbances and additive noise, according to the recent trend in literature [10]. Starting from the approach proposed in [11], our idea is to evaluate for the first time the performance of this controller within the space rendezvous scenario both in simulation, for a three degree-of-freedom (DoF) orbital simulator, and in an experimental setup, i.e. in a three DoF air-bearing spacecraft testbed. Hence, a real-time implementation of the TRMPC approach is here proposed to test the effectiveness of the controller on board.

In order to reach a reasonable computational effort for the robust approach, a time-varying control law is adopted where the feedback gain matrix is evaluated offline. A Linear Matrix Inequalities (LMI) approach is applied to the state feedback stabilization criterion for the stability analysis and the evaluation of the feedback matrix. As explained in [12] and in [13], the proposed method improves the computational efficiency of a robust MPC even using low-thrust propulsion, typically adopted in the final phase of RVD maneuver, as in the proposed case-study. Furthermore, due to the presence of parametric physical uncertainties and discrepancies between the mathematical model and the actual dynamics of the physical system in operation, as non linearities and neglected high-order dynamics, the LMI approach is able to reduce the computational effort required by other robust controller, guaranteeing the stability of the system and improving real-time implementation feasibility. The modeled uncertainties are related to the model linearization of the Hill-Clohesy-Wiltshire (HCW) equations, in which the coupling between the position and speed variables and the quadratic terms related to the distance between the Target and the chaser are neglected. In detail, all the terms  $o(\rho^2/R^2)$  are not considered, with  $\rho$  the distance between the two spacecraft and  $R$  the distance between the Target and the Earth [14]. Moreover, the uncertainties of the control matrix are related to the mass and inertia variation due to the fuel consumption. The LMI approach applied to the Edge Theorem, generalization of the Kharitonov Theorem, allows the offline definition of the feedback gain matrix, which is adopted to define the time-varying control law. Further information of both Edge Theorem and Kharitonov Theorem can be found in [16]. Finally, the robust TRMPC is compared with a classical LQMPC in terms of computational cost, fuel consumption, and constraints satisfaction when the system is affected by persistent bounded uncertainties. The LQMPC, proposed in this paper, was deeply validated in [15], in which a LQMPC and inverse dynamics in the virtual domain (IDVD) guidance methods are combined.

An extensive verification campaign, both in simulation and in an experimental testbed, has been accomplished to validate the performance of the TRMPC. Its compatibility for real-time implementation and constraint satisfaction has been verified when the system is affected by bounded additive disturbances. As said before, the simulations are carried out on a three DoF orbital simulator. Instead, the experimental verification has been carried out using two spacecraft that float over a polished granite monolith surface reproducing a quasi-frictionless motion in Spacecraft Robotics Laboratory at the Naval Postgraduate School [17].

The paper is organized as follows. In Section 2 and 3 the model setup, both of the simulation environment (three DoF

and of the experimental testbed) are presented. The control objective and the system dynamics are explained in detail in Section 4. In Section 5 the MPC design is described, focusing on the theory of the TRMPC and how the concept of Tube is introduced and defined, according to a constraint tightening approach. The simulation results obtained with the three DoF orbital simulator are presented in Section 6 while experimental results are described in Section 7, together with a comparison of the performance of LQMPC and TRMPC. Main conclusions are drawn in Section 8.

*Notation:* The notation employed is standard. Blackboard boldface letters (e.g.,  $\mathbb{X}$ ) denote sets. Bold letters, e.g.,  $\mathbf{u}_k = [u_{0|k} \cdots u_{N-1|k}]$ , are used to denote the stack vector of  $N$  predicted values. Positive (semi)definite matrices  $\mathbf{A}$  are denoted as  $\mathbf{A} \succ 0$  ( $\mathbf{A} \succeq 0$ ), whereas negative (semi)definite matrices are denoted as  $\mathbf{A} \prec 0$  ( $\mathbf{A} \preceq 0$ ). The set  $\mathbb{I}_{\geq 0}$  denotes the positive integers, including 0. We use  $\mathbf{x}_k$  for the (measured) state at time  $k$  and  $\mathbf{x}_{i|k}$  for the state predicted  $i$  steps ahead at time  $k$ .  $\mathbf{A} \oplus \mathbf{B}$  and  $\mathbf{A} \ominus \mathbf{B}$  denotes the Minkowski sum and Pontryagin set difference, respectively.

## 2. Model of the translational three DoF relative orbital maneuver

The nominal relative motion of the two spacecraft in neighboring orbits can be described through HCW linearized equations in the typical continuous-time state-space formulation as  $\dot{\mathbf{x}} = \mathbf{A}\mathbf{x} + \mathbf{B}\mathbf{u}$ , where  $\mathbf{x} = [x, y, z, \dot{x}, \dot{y}, \dot{z}]$  is the state vector representing the 3-position and 3-velocity components of the Chaser with respect to the Target in the local coordinate system (Local Vertical Local Horizontal (LVLH) frame),  $\mathbf{u} = [F_x, F_y, F_z]$  is the control vector, expressed in the body reference frame, represented by the control force components applied to the spacecraft through the actuation system. As described in [18], the LVLH coordinate system is centered on the center of mass (CoM) of the Target and the axes are defined as follows: the  $X$  axis ( $V_{bar}$ ) is in the direction of the orbital velocity vector, the  $Y$  axis ( $H_{bar}$ ) is in the opposite direction of the angular momentum vector of the orbit, while the  $Z$  axis ( $R_{bar}$ ) is radial from the spacecraft center of mass to the CoM Earth. The Chaser has the goal to arrive in the proximity of the Target vehicle, considering a V-bar approach within a cone corridor.  $\mathbf{A}$  and  $\mathbf{B}$ , the state and control matrices respectively, are defined as in [19] as a function of the angular velocity of the orbit (known and constant) with respect to the inertial frame  $\omega_0$  and the wet mass of the Chaser  $m_{CV}$ .

Due to the space environment, external disturbances in terms of forces and moments, such as the J2, the gravity gradient, and the solar radiation pressure, could affect the vehicle performance and drive the chaser to violate the constraints. If these additive noises are included in the spacecraft dynamics, the following continuous-time uncertain system shall be considered

$$\dot{\mathbf{x}} = \mathbf{A}\mathbf{x} + \mathbf{B}\mathbf{u} + \mathbf{B}_w \mathbf{w}, \quad (1)$$

where  $\mathbf{w}$  is the vector of persistent noise, mainly related to the external environment and can be modeled as a random and bounded noise. In particular, the disturbance sequence is the realization of a stochastic process where  $\mathbf{w} \in \mathbb{W}$  is a random variable with known distribution, and the set  $\mathbb{W}$  is a compact

and convex set, containing the origin in its interior. Then, a discrete-time representation of system (1) is derived as follows

$$\mathbf{x}_{k+1} = \mathbf{A}_d \mathbf{x}_k + \mathbf{B}_d \mathbf{u}_k + \mathbf{B}_{w_d} \mathbf{w}_k, \quad (2)$$

162 where  $\mathbf{A}_d$ ,  $\mathbf{B}_d$ , and  $\mathbf{B}_{w_d}$  are the discrete matrices correspond-  
 163 ing to the continuous ones in (1). A goal of the control is to  
 164 drive the system to the docking position, compliant with the  
 165 constraints satisfaction in terms of position and velocity during  
 166 the proximity maneuver. In a typical cone-approach maneuver  
 167 (see Figure 1), the Chaser should lie within the projection of  
 168 the approach cone in the  $x-z$  orbital plane. As shown in Figure  
 169 1(a), the Chaser starts the rendezvous maneuver at  $x = x_i$  and  
 170 ends up to  $x = x_f$ , where the docking phase begins. The angle  
 171  $\theta$  defines the approaching truncated cone and is a function of  
 172 the cone bases radius, i.e. the initial one  $r_i$  and  $r_f$ . In Figure  
 173 1(b), the constraints in the  $y-z$  plane are represented with re-  
 174 spect to the section  $A-A$  identified in Figure 1(a). As we can  
 175 notice, the constraint set for the position along  $y$  is fixed and  
 176 equal to  $[y_{min}, y_{max}] = [-r_f, r_f]$  whereas, in compliance with  
 177 Figure 1(a), the constraints along  $z$  are time-varying, since the  
 178 radius of the cone decreases from  $r_i$  at  $z = z(x_i)$  (black dashed  
 179 rectangle) to  $r_f$  at  $z = z(x_f)$  (green dashed rectangle).

The related position boundaries can be expressed as follows

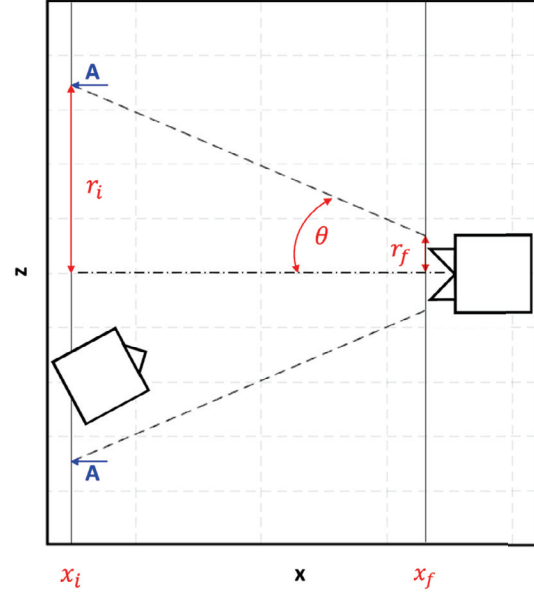
$$\begin{aligned} x_i &\leq x \leq x_f, \\ -r_f &\leq y \leq r_f, \\ |z| &\leq (x_f - x) \tan \theta - (r_i - r_f), \end{aligned}$$

180 whereas the velocity constraints are defined in order to bound  
 181 each velocity components norm to be less or equal to the maxi-  
 182 mum one, defined for the maneuver. Hard constraints are con-  
 183 sidered also on the input, in order to be compliant with the  
 184 saturation of the actuation system. The input constraint set  
 185 is defined according to the maximum level of thrust that the  
 186 actuators can provide.

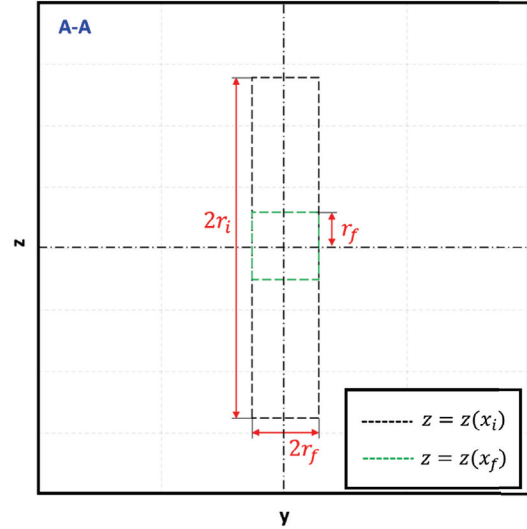
### 187 3. Model of the planar experimental testbed

188 The two controllers, the TRMPC as well as the LQMPC  
 189 for comparison reasons, are experimentally tested on the Naval  
 190 Postgraduate School (NPS) Proximity Operation of Spacecraft:  
 191 Experimental hardware-In-the-loop DYNAMIC simulator (PO-  
 192 SEIDYN) testbed. The NPS-POSEIDYN testbed consists of  
 193 Floating Spacecraft Simulators (FSS), a polished granite mono-  
 194 lith, a Vicon motion capture system, and a ground station com-  
 195 puter. Figure 2 shows an overview of the testbed.

196 The floating surface is a 15 ton, 4-by-4 meter granite mono-  
 197 lith, with a planar accuracy of  $\pm 0.0127$  mm and a horizontal  
 198 leveling accuracy of less than 0.01 deg. The FSSs float over the  
 199 granite surface via three flat air bearings. The quasi-frictionless  
 200 environment with the low residual acceleration of the FSS em-  
 201 ulates the environment in space. The FSS has eight cold gas  
 202 thrusters fed by compressed air from an on-board tank [20].  
 203 Using the on-board computer the FSS is able to perform real-  
 204 time computation of guidance and control algorithms. The Vi-  
 205 con motion capture system, composed of ten overhead cameras  
 206 that track reflectors mounted on the FSS, provides accurate  
 207 position and orientation data. These data are streamed to the  
 208 FSS using a Wi-Fi connection. They are then augmented with  
 209 angular velocity measurements provided by an on-board fiber-  
 210 optic gyroscope. A discrete Kalman filter processes the data



(a)  $x-z$  orbital plane



(b)  $y-z$  normal-to-orbit plane

Figure 1: Cone approach for 3DoF Orbital Simulator.

211 and provides a full state estimate. Detailed description of the  
 212 NPS-POSEIDYN testbed can be found in [17].

213 The FSS dynamic model consists of three double integra-  
 214 tors, two translational and one rotational DoF. The discrete-  
 215 time dynamics in the presence of additive disturbances is de-  
 216 scribed in a state-space formulation as (1), with the discrete-  
 217 time state, control, and disturbance matrices corresponding to  
 218 the continuous ones reported below



Figure 2: NPS-POSEIDYN testbed with the Vicon motion capture cameras, FSSs, and granite monolith in the Spacecraft Robotics Laboratory at the Naval Postgraduate School. The Target FSS is on the right and the Chaser FSS is on the left.

$$\mathbf{A} = \begin{bmatrix} \mathbb{0}_{3 \times 3} & \mathbb{I}_3 \\ \mathbb{0}_{3 \times 3} & \mathbb{0}_{3 \times 3} \end{bmatrix}, \quad \mathbf{B} = \begin{bmatrix} \mathbb{0}_{3 \times 3} \\ \frac{1}{m} & 0 & 0 \\ 0 & \frac{1}{m} & 0 \\ 0 & 0 & \frac{1}{I_z} \end{bmatrix}, \quad \mathbf{B}_w = \mathbb{I}_6, \quad (3)$$

where  $m$  and  $I_z$  are the mass and moment of inertia about the vertical axis of the FSS, respectively.

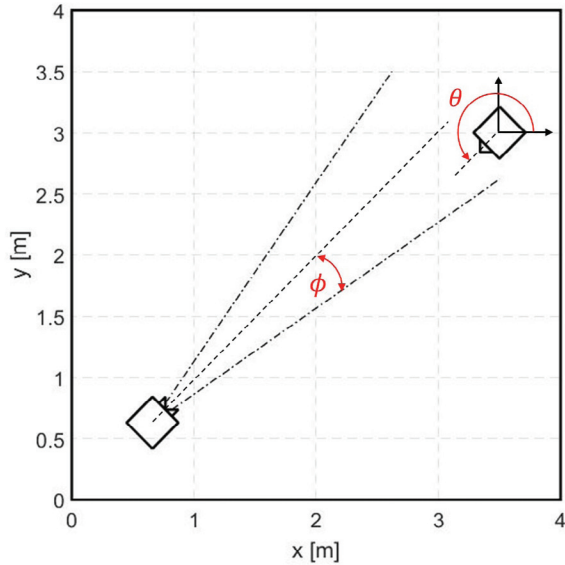


Figure 3: Cone approach for 3DoF NPS-POSEIDYN testbed.

The Chaser FSS is constrained to lie within a cone (see Figure 3) and the related boundaries are translated in position constraints as

$$\begin{aligned} x_T &\leq x \leq x_T + x_i \sqrt{2} \cos\left(\frac{\pi}{4} \pm \phi\right) / \cos \phi, \\ y_T &\leq y \leq y_T + x_i \sqrt{2} \sin\left(\frac{\pi}{4} \pm \phi\right) / \cos \phi, \end{aligned}$$

where  $\phi$  is the cone angle and  $(x_T, y_T)$  are the final position of the FSS Chaser, corresponding to the FSS Target position. Bounded constraints are also introduced for the velocity components and the relative attitude, as described in Section 5.

The polytope set for the additive disturbance has to be defined. Hence, the persistent uncertainty has been evaluated first through simulations, and then the results have been validated experimentally with respect to the testbed environment. According to the specifications of the cold gas thrusters, a random error related to the thrust magnitude has been taken into account, considering a  $\pm 10\%$  error over the maximum thrust level available. Then, the same mission profile has been simulated two times. First, both the external environment and the actuation system have been considered ideal, i.e., not affected by disturbance. Next, the simulation has been repeated considering noise from the environment and random error affecting the thrusters. Hence, the states evolutions have been compared, in order to size the maximum disturbance level that can affect the system. Then, these results have been later validated with the characterization of the testbed, performing several experiments, considering same initial conditions.

#### 4. System dynamics and control objective

Let consider a generic model of the form (2), where the noise is a realization of a stochastic process, each one an independent and identically distributed (i.i.d.), zero-mean random variable, with bounded and convex support  $\mathbb{W} \in \mathbb{R}^n$ , containing the origin in its interior.

The system is subject to hard constraints on both the state and input of the form

$$\mathbf{x} \in \mathbb{X}, \quad \mathbf{u} \in \mathbb{U}, \quad (4)$$

where  $\mathbb{X}$  and  $\mathbb{U}$  are polytope.

To solve the control problem, a robust MPC algorithm is considered [11], repeatedly solving the following optimal control problem where the finite horizon quadratic cost  $J_N(\mathbf{x}, \mathbf{u})$  to be minimized at the current time  $k$  is

$$J_N(\mathbf{x}_k, \mathbf{u}_k) = \sum_{i=0}^{N-1} (\mathbf{x}_{i|k}^T \mathbf{Q} \mathbf{x}_{i|k} + \mathbf{u}_{i|k}^T \mathbf{R} \mathbf{u}_{i|k}) + \mathbf{x}_{N|k}^T \mathbf{P} \mathbf{x}_{N|k}, \quad (5)$$

where  $\mathbf{Q} \in \mathbb{R}^{n \times n}$ ,  $\mathbf{Q} \succ 0$ ,  $\mathbf{R} \in \mathbb{R}^{m \times m}$ ,  $\mathbf{R} \succ 0$ , and  $\mathbf{P}$  is the solution of the discrete algebraic Riccati equation.

Due to the presence of a bounded and persistent unknown disturbance  $w$ , the state of the system

$$\mathbf{x}_{i|k} = \mathbf{z}_{i|k} + \mathbf{e}_{i|k} \quad (6)$$

can be split into a nominal part,  $\mathbf{z}_{i|k}$ , and an error part,  $\mathbf{e}_{i|k}$ , which represents the deviation of the actual state  $\mathbf{x}_{i|k}$  with respect to the nominal one. Applying the following feedback policy

$$\mathbf{u}_{i|k} = \mathbf{v}_{i|k} + \mathbf{K}(\mathbf{x}_{i|k} - \mathbf{z}_{i|k}), \quad (7)$$

267 where the matrix  $\mathbf{K}$  is chosen so that  $\mathbf{A}_K = \mathbf{A} + \mathbf{B}\mathbf{K}$  is Schur  
 268 stable, then the corresponding nominal and error dynamics can  
 269 be described respectively by

$$z_{i+1|k} = \mathbf{A}z_{i|k} + \mathbf{B}v_{i|k}, \quad z_{0|k} = x_{0|k}, \quad (8)$$

$$e_{i+1|k} = \mathbf{A}_K e_{i|k} + \mathbf{B}_w w_{i|k}, \quad e_{0|k} = 0. \quad (9)$$

270 Hence, the finite horizon optimal quadratic cost (5) can be  
 271 re-defined in terms of nominal state  $z_k$  and control input  $\mathbf{v}_k$  as

$$J_N(z_k, \mathbf{v}_k) = \sum_{i=0}^{N-1} (z_{i|k}^T \mathbf{Q} z_{i|k} + v_{i|k}^T \mathbf{R} v_{i|k}) + z_{N|k}^T \mathbf{P} z_{N|k}, \quad (10)$$

272 and the related finite horizon optimal control problem can be  
 273 reformulated as follows.

274 **Definition 1** (Nominal Finite Horizon Optimal Control  
 275 Problem) *Given the nominal system dynamics (8), cost (10)  
 276 and nominal constraints set  $\mathbb{Z}$ ,  $\mathbb{V}$ , and  $\mathbb{Z}_f$ , the nominal Robust  
 277 MPC finite horizon optimization problem is*

$$\min_{\mathbf{v}} J_N(z_k, \mathbf{v}_k) \quad (11a)$$

$$\begin{aligned} \text{s.t. } & z_{i+1|k} = \mathbf{A}z_{i|k} + \mathbf{B}v_{i|k}, \quad z_{0|k} = x_k, \\ & z_{i|k} \in \mathbb{Z}, \quad i \in [1, N], \\ & v_{i|k} \in \mathbb{V}, \quad i \in [0, N-1], \\ & z_{N|k} \in \mathbb{Z}_f. \end{aligned} \quad (11b)$$

The solution of (11) is the optimal nominal control sequence  $\mathbf{v}_{0|k}^*(z_k) = [v_{0|k}^*(0; z_k), \dots, v_{T-1|k}^*(T-1; z_k)]$  and the first control action, i.e.,  $\tilde{\kappa}_N(z_k) := v_{0|k}^*(0; z_k)$ , represents the optimal control to be applied. The correspondent control applied on the uncertain system, according to the control policy adopted, is

$$\kappa_N(x_k, z_k) = \tilde{\kappa}_N(z_k) + \mathbf{K}(x_k - z_k). \quad (12)$$

279 The composite close-loop system then satisfies

$$\begin{aligned} x_{i+1|k} &= \mathbf{A}x_{i|k} + \mathbf{B}\kappa_N(i, x_k, z_k) + \mathbf{B}_w w_{i|k}, \\ z_{i+1|k} &= \mathbf{A}z_{i|k} + \mathbf{B}\tilde{\kappa}_N(i, z_k). \end{aligned} \quad (13)$$

280 For the TRMPC approach, considering discrete-time Linear  
 281 Time Invariant (LTI) formulation of the system and the control  
 282 policy defined in Eq. (7), the  $\mathbf{K}$  matrix is defined to stabilize  
 283 the system. The stability analysis has been performed consider-  
 284 ing the application of the LMI approach to the state feedback  
 285 stabilization criterion, applying the definition of Schur stability  
 286 to the closed-loop system

$$x_{i+1|k} = (\mathbf{A} + \mathbf{B}\mathbf{K})x_{i|k} + \mathbf{B}v_{i|k} + \mathbf{B}_w w_{i|k}, \quad (14)$$

287 Hence, the satisfaction of the following condition aims to define  
 288 the feedback gain matrix  $\mathbf{K}$  that stabilize the system

$$(\mathbf{A} + \mathbf{B}\mathbf{K})^T \hat{\mathbf{P}} (\mathbf{A} + \mathbf{B}\mathbf{K}) - \hat{\mathbf{P}} \prec 0, \quad \hat{\mathbf{P}} \succ 0. \quad (15)$$

289 Adopting a feedback linearization control strategy implies the  
 290 definition of a state feedback control law able to overcome sys-  
 291 tem nonlinearities and, at the same time, to impose some de-  
 292 sired linear dynamics. On the other hand, the control scheme  
 293 success is strongly dependent on how much the model descrip-  
 294 tion of the system under consideration fit with the real physical  
 295 system in operation. Hence, linearizing the system dynamics

means introducing in the plant parametric uncertainties represent-  
 296 ing the discrepancies between the mathematical model  
 297 and the actual dynamics, in terms of neglected nonlinearities,  
 298 unmodeled high-frequency dynamics, and deliberate reduced-  
 299 order models. Furthermore, additional parametric uncertain-  
 300 ties are represented by system-parameters variations due to  
 301 environmental and/or physical changes. All these errors intro-  
 302 duced in the model have to be considered since they might affect  
 303 the performance as well as the stability of the control system.  
 304 Therefore, a stability analysis must be performed in which param-  
 305 etric uncertainties related to the application studied are explic-  
 306 itly considered. In this work, the stability analysis has been  
 307 evaluated through an LMI approach applied to the well-known  
 308 Edge Theorem, which is an extension of Karitonov's theorem  
 309 ([16]) and states that the stability of a polytope of polynomi-  
 310 als can be guaranteed by the stability of its one-dimensional  
 311 exposed edge polynomials [21]. The Edge Theorem takes into  
 312 account the dependence of the polynomial coefficients on the  
 313 uncertain parameters and the coefficients of the polynomials are  
 314 affine functions of the uncertain vector  $q = [q_1, \dots, q_l]$ , bounded  
 315 in the hyper-rectangle  $B_q$  defined by

$$B_q := \left\{ q \in \mathbb{R}^l \mid q_i \in [q_i^-, q_i^+], i = 1, \dots, l \right\}. \quad (16)$$

**Theorem 1** (*Edge Theorem*) Consider the polytope of poly-  
 nomials  $\tilde{P}$ , defined as

$$\begin{aligned} \tilde{P} &= \left\{ p(s, q) = a_0(q) + a_1(q)s + \dots + a_{n-1}(q)s^{n-1} + s^n \right. \\ &\quad \left. : a_i(q) = a_{i_0} + \sum_{k=1}^l a_{i_k} q_k, q \in B_q, \quad i = 0, \dots, n-1 \right\}. \end{aligned} \quad (17)$$

The family  $\tilde{P}$  is Hurwitz if and only if all edges of  $\tilde{P}$  are Hurwitz  
 (see [22]). Starting from the discrete nominal state and control  
 matrices,  $\mathbf{A}_d$  and  $\mathbf{B}_d$ , the corresponding uncertain matrices are  
 defined as  $\mathbf{A}_d^- = \mathbf{A}_d(q^-)$ ,  $\mathbf{A}_d^+ = \mathbf{A}_d(q^+)$ ,  $\mathbf{B}_d^- = \mathbf{B}_d(q^-)$ , and  
 $\mathbf{B}_d^+ = \mathbf{B}_d(q^+)$ .

Then, a system of four LMI is defined to solve a joint sta-  
 bilization problem based on the Edge Theorem and Lyapunov  
 stability condition, coupling the uncertain matrices defined be-  
 fore. The feedback matrix  $\mathbf{K}$ , used to define a time-varying  
 control law, is derived through this approach and ensures the  
 stability of the system for every modeled uncertainty that may  
 affect the system itself.

In this work, the adopted linearized dynamics of the Chaser  
 spacecraft relative to the Target vehicle during the final ap-  
 proach of the rendezvous maneuver has been derived by Clo-  
 hessy and Wiltshire in [14], starting from the nonlinear equa-  
 tions for the restricted three-body problem and considering for  
 the both the spacecraft a reference circular orbit around a mas-  
 ter body. Considering the two spacecraft mass infinitesimal  
 with respect to the mass of the main body and defining  $\rho = \rho_1 \rho$   
 and  $r_1 = r_1 \mathbf{i}_\xi$  as the position vectors of the Chaser and the  
 Target spacecraft respectively, and with  $r = r \mathbf{i}_\xi$  the vectorial  
 sum of the two positions,  $r = \rho + r_1$ , the equations of motion of  
 the Chaser spacecraft can be rewritten as

$$\frac{d^2 \rho}{dt^2} + 2\omega \times \frac{d\rho}{dt} + \omega \times [\omega \times (\rho + r_1)] = -\frac{\omega^2 r_1^3}{r^3} \mathbf{r}, \quad (18)$$

where  $\omega$  is the orbital angular rate. This differential equation  
 presents nonlinearities due to the term  $1/r^3$ . As described in

[14], the use of a Taylor Series expansion allows to obtain a linear equation if we ignore the higher order terms, i.e.  $O(\rho^2/r_1^2)$  as  $\frac{r_3^3}{r_1^3} = 1 - 3i_\xi \cdot i_\rho \frac{\rho}{r_1} + O(\frac{\rho^2}{r_1^2})$ . Then, Eq. (18) reduces to

$$\frac{d^2\rho}{dt^2} + 2\omega \times \frac{d\rho}{dt} + \omega \times (\omega \times \rho) = -\omega^2 \rho + 3\omega^2 (i_\xi \cdot \rho) i_\xi + O(\rho^2). \quad (19)$$

We finally get the linearized differential equation for the motion of the Chaser relative to the Target spacecraft as

$$\frac{d^2\rho}{dt^2} + 2\omega \times \frac{d\rho}{dt} = -\omega^2 \zeta i_\zeta + 3\omega^2 \xi (i_\xi + O(\rho^2)). \quad (20)$$

Ignoring the  $O(\rho^2)$  and expressing the position vector in a more convenient way as

$$\rho \equiv \mathbf{r} = x i_\theta + z i_r - y i_y, \quad i_{r_1} = i_r \quad \omega = -\omega i_y, \quad (21)$$

with  $x$  in the direction of the motion  $i_\theta$ ,  $z$  in the radial direction  $i_r$ , and  $i_y = i_\theta \times i_r$  normal to the orbital plane. Then, we can obtain the scalar form of Eq. (19), which is the well-known HCW Equation. Hence, the parametric uncertainty introduced in the model are of the same order of  $O(\rho^2/r_1^2)$  and  $O(\rho^2)$ . When external forces are acting on the system, in this case due to the correction actions actuated by the thrusters ( $F_x, F_y, F_z$ ) of the AOCS subsystem, we have

$$\begin{aligned} \frac{d^2x}{dt^2} - 2\omega \frac{dz}{dt} &= \frac{F_x}{m_{CV}}, \\ \frac{d^2y}{dt^2} + \omega^2 y &= \frac{F_y}{m_{CV}}, \\ \frac{d^2z}{dt^2} + 2\omega \frac{dx}{dt} - 3\omega^2 z &= \frac{F_z}{m_{CV}}. \end{aligned} \quad (22)$$

Therefore, additional uncertainties have been introduced in terms of minimal physical changes of the Chaser spacecraft mass  $m_{CV}$  during the maneuver as well as environmental impact on the orbital angular velocity  $\omega$ . Furthermore, for what concern the experimental setup, additional simplifications have been introduced, since the Chaser FSS dynamics is represented by only three double integrators, ignoring the coupling between the two translational DoFs and the angular velocity, and the inertia with respect to the axis normal to the motion is considered for the rotational dynamics, implying new physical uncertainties. All these errors have been taken into account for the stability analysis and the evaluation of the feedback gain matrix, which has been derived offline, reducing the computational effort usually required to robust controllers and allowing the real-time implementation.

## 5. Tube-based robust MPC approach

### 5.1. Definition of tube-based approach

In order to robustly satisfy the mission constraints, they are tightened to allow the trajectories of the uncertain system, affected by disturbance, to lie in a tube centered on the nominal one, where each trajectory is related to a particular realization of the uncertainty at each time step  $k$ . In this Section, the derivation of the nominal state, input, and terminal constraints set  $\mathbb{Z}$ ,  $\mathbb{V}$ , and  $\mathbb{Z}_f$  are described according to the approach proposed in [11], so that the constraints (4) of the system (2) are satisfied for every realization of the disturbance sequence  $\mathbf{w}$ , by suitable design of the tube.

Let define  $S_K(\infty) := \sum_{j=0}^{\infty} \mathbf{A}_K^j \mathbb{W}$ , the uncertain set of the error  $\mathbf{e}_{i|k}$ , as the minimal robust positive invariant set for  $\mathbf{x}_{i+1|k} = \mathbf{A}_K \mathbf{x}_{i|k} + \mathbf{B}_K \mathbf{w}_{i|k}$ ,  $\mathbf{w} \in \mathbb{W}$ . Then, the state and control constraints are satisfied if

$$\begin{aligned} \mathbf{z}_{i|k} &\in \mathbb{X} \ominus S_K(\infty), \\ \mathbf{v}_{i|k} &\in \mathbb{U} \ominus \mathbf{K} S_K(\infty). \end{aligned} \quad (23)$$

Satisfaction of the terminal constraint at time instant  $N$  for the uncertain system (2) is ensured if the nominal system satisfies the *tighter* constraint

$$\mathbf{z}_N \in \mathbb{Z}_f \subseteq \mathbb{X}_f - S_K(\infty), \quad \mathbb{Z}_f \subseteq \mathbb{Z}. \quad (24)$$

These assertions only make sense if the disturbance set  $\mathbb{W}$  is sufficiently small to satisfy the following Assumption 1, as defined in [11].

**Assumption 1** (*Restricted disturbances for constraints satisfaction*)  $S_K \subset \mathbb{X}$  and  $\mathbf{K} S_K \subset \mathbb{U}$ .

The next step consists in the definition of a robust positively invariant set  $S_K$  for (9) to obtain the tighter constraints acting on the nominal system. Then the constraints are considered for the TRMPC problem. Several methods can be adopted, as proposed in [23], [24], and [25]. Once the uncertainty set  $\mathbb{W}$  is evaluated, an inner approximation of the nominal constraint set is defined, according to the following strategy presented in [11]:

1. Consider a single linear constraint as

$$\mathbb{X} = \{ \mathbf{x}_{i|k} \in \mathbb{R}^n \mid a \mathbf{x}_{i|k} \leq b \}. \quad (25)$$

2. Since  $\mathbf{x}_{i|k} = \mathbf{z}_{i|k} + \mathbf{e}_{i|k}$  for all  $i \in \mathbb{I}_{\geq 0}$ , where  $\mathbf{e}_{i|k} \in S_K(\infty)$ , it follows that

$$a \mathbf{z}_{i|k} \leq b - \max \{ a \mathbf{e}_{i|k} \mid \mathbf{e}_{i|k} \in S_K(\infty) \} = b - \Phi_\infty. \quad (26)$$

3. Compute an upper approximation of  $\Phi_\infty$  as

$$\Phi_N = \max \left\{ a \sum_{i=0}^{N-1} \mathbf{A}_K^i \mathbf{w}_{i|k} \mid \mathbf{w}_{i|k} \in \mathbb{W} \right\}. \quad (27)$$

4. Considering the feedback control matrix  $\mathbf{K}$  and the prediction horizon  $N$ ,  $\mathbf{A}_K^N \in \alpha \mathbb{W}$  with  $\alpha \in (0, 1)$ . We then obtain

$$\Phi_\infty \leq (1 - \alpha)^{-1} \Phi_N. \quad (28)$$

5. Hence, the constraint set  $\mathbb{Z}$  can be defined as

$$\mathbb{Z} := \{ \mathbf{z}_{i|k} \in \mathbb{R}^n \mid a \mathbf{z}_{i|k} \leq b - (1 - \alpha)^{-1} \Phi_N \}. \quad (29)$$

Analogous procedure has been used to obtain a suitable control constraint set  $\mathbb{V}$ .

### 5.2. Tube-based robust MPC algorithm

Once the tube is defined in order to contain all the trajectories of an uncertain system subject to additive disturbances, an optimal control problem can be formulated. The solution of the problem provides a control policy that minimizes a quadratic cost. The solution also ensures that the state and control constraints are satisfied for all admissible bounded disturbance sequences. The application of TRMPC guarantees that the trajectory evolved from the initial state lies within a robust positive invariant set, defined to satisfy state and control constraints acting on the system, allowing to control the uncertain system (2) by constraining its trajectory to lie within a

434 tube whose center is the solution of the nominal system (8)  
 435 obtained applying the implicit MPC control law  $\tilde{\kappa}_N(z_k)$ . The  
 436 final TRMPC algorithm can be divided into two parts: (i) an  
 437 offline computation of the feedback matrix  $\mathbf{K}$ , which stabilizes  
 438 the system (described in detail in Section 4), and of the tight-  
 439 ened constraints set  $\mathbb{Z}$  and  $\mathbb{V}$ , as shown in Algorithm 1 and  
 440 Algorithm 2, and (ii) the repeated online optimization prob-  
 441 lem, i.e., Algorithms 3.

---

#### Algorithm 1 Constraint Tightening

---

```

1: procedure CONSTRAINT TIGHTENING
2:   Define  $\mathbb{X}$ ,  $\mathbb{U}$ , and  $\mathbb{W}$ 
3:   Set  $\alpha \in (0, 1)$ 
4:   Evaluate  $\mathbb{N}$  subject to  $\mathbf{A}_K^N \in \alpha\mathbb{W}$ 
5:   Compute  $\Phi_N$ 
6:   Evaluate  $\mathbb{Z}$ ,  $\mathbb{V}$  and  $\mathbb{Z}_f$ 
7: end procedure

```

---



---

#### Algorithm 2 Feedback Gain Evaluation

---

```

1: procedure
2:   Define  $B_q$  as in (16)
3:   Build  $(\mathbf{A}_i, \mathbf{B}_i)_{q \in \text{supp}(B_q)}$ 
4:   for each  $i$ -th vertex  $(\mathbf{A}^i, \mathbf{B}^i)$  do
5:     Build  $(\mathbf{A}_i, \mathbf{B}_i)_{q \in \text{supp}(B_q)}$ 
6:      $\text{sys}_i = \mathbf{X} \mathbf{A}_i^T + \mathbf{A}_i^T \mathbf{X} - \mathbf{Y}^T \mathbf{B}_i^T - \mathbf{B}_i^T \mathbf{Y}$ 
7:   end for
8:   Solve  $[\mathbf{X} \succ 0, \text{sys}_i \prec 0]$ 
9:   Get  $\mathbf{X}$  and  $\mathbf{Y}$ 
10:  Get  $\mathbf{K} = \mathbf{Y} \mathbf{X}^{-1}$ 
11: end procedure

```

---



---

#### Algorithm 3 TRMPC Algorithm

---

```

1: procedure
2:   Set  $N$ 
3:   At current time  $k$  for  $i = 0$ , evaluate  $x_{i=0|k} = x_k$ 
4:   for  $i = 0 : N - 1$  do
5:     Set  $z_{i=0|k} = z_0 = x_k$ 
6:     Solve (11)
7:   end for
8:   Get  $\mathbf{v}_0(z_0)$ 
9:   Get  $v_0(0; z_0)$  and evaluate  $z_{k+1}$  applying  $v_0(0; z_0)$   

  on Eq. (8)
10:  Evaluate  $u_k$  according to Eq. (7), then evaluate  

 $x_{k+1}$  applying  $u_k$  on Eq. (2)
11: end procedure

```

---

## 6. Simulation results

443 The LQMPC approach has been already validated in a sim-  
 444 ulation environment, as described in [6], where it has been  
 445 shown how this approach can effectively handle various con-  
 446 straints arising in rendezvous and proximity operations in the  
 447

orbital plane. ESA's ORCSAT project [26] has investigated  
 the adoption of LQMPC on the Mars Sampling Return cap-  
 ture scenario. Moreover, LQMPC has already been tested in  
 space by PRISMA project to demonstrate Guidance, Naviga-  
 tion, and Control (GNC) strategies for spacecraft formation  
 flying and rendezvous, considering a classical MPC control for  
 fuel saving based on orbit propagation [27]. On the other hand,  
 these studies do not consider the robustness of the controller to  
 persisting disturbances due to several sources that can strongly  
 affect the spacecraft and may bring the chaser to collide with  
 the target.

In [8], both classical and robust MPC (not TRMPC) have  
 been adopted to solve the problem of RVD of spacecraft, using  
 the HCW model where additive disturbances affect the system  
 during the maneuver. The results show the classical MPC is  
 not able to handle disturbances. Hence, in this section the sim-  
 ulation results related to the application of an LQMPC in the  
 presence of persistent disturbances will not be reported. On  
 the other hand, a different robust approach with respect to [8],  
 i.e., TRMPC approach, has been implemented into a MAT-  
 LAB/Simulink three DoF orbital simulator to show how the  
 chosen controller is able to handle the persisting uncertainties  
 due to the external environment and still robustly satisfy the  
 mission and system constraints. In this Section, we briefly show  
 the results related to the application of the TRMPC approach  
 to the three DoF system translational dynamics. The system of  
 the form of (2) is affected by persistent bounded disturbances,  
 related to three main causes: (i) Earth-oblateness resulting in  
 an asymmetric gravity potential  $J_2$  term and a gravity gradi-  
 ent effect; (ii) drag due to the residual atmosphere; (iii) solar  
 radiation pressure. The other environmental effects due to  
 third-bodies or disturbances due to thrusters plume interac-  
 tions are neglected because of the lower impact on the system.  
 Hence, the set of additive disturbance considered is defined as  
 $w \in \mathbb{W} = \{w \mid \|w\|_\infty \leq 10^{-2}\}$ . The system is subject to hard  
 constraints on both states and inputs. The uncertain sets have  
 been introduced in Section 2. The cone geometry and the defin-  
 ing parameters are reported in Table 1, whereas the tightened  
 constraints are reported in Table 2.

Table 1: Cone geometry and mission scenario definition.

Parameter	Value
$x_i$	350 [m]
$x_f$	0 [m]
$r_i$	7 [m]
$r_f$	0.1 [m]
$\theta$	10 [deg]

Table 2: 3DoF State and Control tightened constraints.

Parameter	Nominal System Value
$F_{max}$	$[-0.99, 0.99]$ [N]
$(x_{min}, x_{max})$	$[-349.97, 4.97]$ [m]
$(z_{min}, z_{max})$	$[-6.97, 6.97]$ [m]
$(y_{min}, y_{max})$	$[-0.07, 0.07]$ [m]
$V_x, V_y, V_z$	$[-0.12, 0.12]$ [m/s]

The Chaser vehicle is modeled as a cubic-shape spacecraft  
 (1.2 m side) with a mass of 600 kg and equipped with six

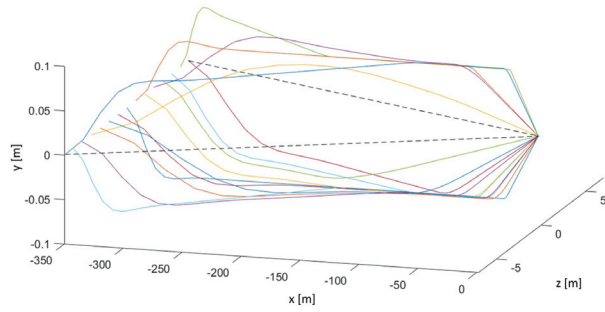


Figure 4: TRMPC nominal simulated trajectories for different initial conditions.

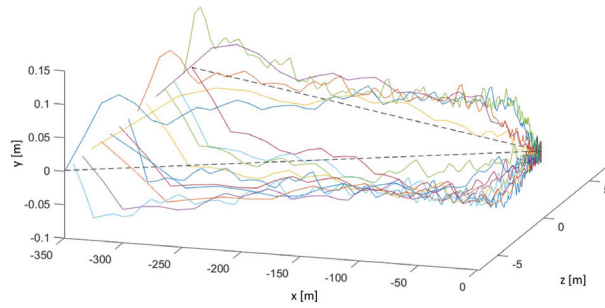


Figure 5: TRMPC uncertain simulated trajectories for different initial conditions.

489 thrusters, two along each body axis and in two different ori-  
 490 entation, each with a specific impulse of  $I_{sp} = 220$  s and a  
 491 maximum thrust of  $F_{max} = 1$  N. The reference scenario sees  
 492 the Chaser and the Target in a Low Earth Orbit with an alti-  
 493 tude of 650 km, at an initial relative distance of  $-350$  m along  
 494 the V-bar axis. Moreover, the active vehicle has a residual  
 495 velocity of  $0.05$  m/s with respect to the passive one.

496 The diagonal matrices  $\mathbf{Q}$  and  $\mathbf{R}$  are set to  $10^2 \times \mathbb{I}_6$  and  $\mathbb{I}_3$ ,  
 497 respectively, while  $\mathbf{P}$  is the solution of the discrete Algebraic  
 498 Riccati equation. Furthermore, simulation settings are listed  
 499 in Table 3.

Table 3: 3DoF MPC design parameters and model initialization settings.

Parameter	Value
MPC Sample Time	1 [s]
Prediction Horizon	10
System Sample Time	1 [s]

500 To show the effectiveness of the TRMPC approach for the  
 501 last phase of a space rendezvous maneuver, a set of simula-  
 502 tions considering different Initial Conditions (ICs) within the  
 503 entry cone have been performed considering a minus V-bar ap-  
 504 proach, in order to highlight the performance of the controller  
 505 for each initial state vector within the state constraint set  $\mathbb{X}$ .  
 506 Figure 4 represents the 3D nominal and disturbed trajectories,  
 507 respectively. We can see how the mission constraints in terms  
 508 of position are satisfied, both within the cone in the orbital

509 plane and the out-of-plane corridor. Each trajectory is driven  
 510 to converge to the V-bar axis, according to a decreasing pro-  
 511 file of the velocity along the approaching axis and satisfying  
 512 the terminal constraints of null residual velocity between the  
 513 spacecraft. Moreover, comparing the two figures, it is clear how  
 514 the effect of disturbances is perceived strongly in the last part  
 515 of the maneuver, but also in this phase, the proper definition  
 516 of tightened constraints ensure the mission and system con-  
 517 straints satisfaction in the presence of additive disturbances,  
 518 within the prescribed final safe region.

## 7. Experimental results

### 7.1. Scenario initialization

519 In this section, the results related to the application of  
 520 TRMPC to the FSS system dynamics are here presented, to-  
 521 gether with the results obtained applying the LQMPC scheme  
 522 to compare the performance of the two controllers in the pres-  
 523 ence of persistent disturbance. The experimental setup is com-  
 524 posed by two FSSs, one moving representing the Chaser and  
 525 the other one fixed, the Target, each one with a mass of 9.966 kg  
 526 and equipped with a set of eight thrusters of 0.15 N on-board,  
 527 controlled via a Sigma-Delta Modulation method [28]. First,  
 528 the MATLAB/Simulink based numerical simulator that recre-  
 529 ates the whole FSS system, reproducing its dynamics and emu-  
 530 lating the on-board sensors and actuators, is used to validate  
 531 the models and tune the controllers. Then, the experiments  
 532 are conducted on the NPS-POSEIDYN testbed [17]. The FSS  
 533 has an on-board PC-104 computer based on an Intel Atom 1.6  
 534 GHz 32 bit processor with a 2 GB of RAM and an 8 GB solid-  
 535 state drive. The operating system of the on-board computer is  
 536 an RTAI-patched Ubuntu 14.04 Sever Edition which provides  
 537 real-time execution capabilities. The developed LQMPC and  
 538 TRMPC controllers are cross-compiled for the FSS 32-bit ar-  
 539 chitecture and later transferred to the FSS.

540 The discrete-time linearized system is of the form (2), where  
 541 the persistent disturbances affecting the system are defined as  
 542 zero-mean random variables defined in an aforementioned con-  
 543 vex and compact set  $\mathbf{w} \in \mathbb{W} = 10^{-2} \mathbb{I}_6$ .

544 The hard constraints on states and inputs are defined in  
 545 Table 7.1 for the uncertain system, which represent also the  
 546 constraints for the LQMPC setup, together with the tight-  
 547 ened constraints defined for the TRMPC problem. The ma-  
 548

Table 4: State and Control constraints.

Parameter	Uncertain	Nominal
	Value	Value
$F_{max}$	$\pm 0.15$ [N]	$\pm 0.0927$ [N]
$\phi$	10 [deg]	8 [deg]
$\theta$	$\pm 2\pi$ [rad]	$\pm 6.2496$ [rad]
$V_x, V_y$	$\pm 0.2$ [m/s]	$\pm 0.1777$ [m/s]
$\dot{\theta}$	$\pm 0.1$ [rad/s]	$\pm 0.0777$ [rad/s]

549 trices  $\mathbf{Q}$  and  $\mathbf{R}$  are set to  $diag(10^4 \ 10^4 \ 10^0 \ 10^8 \ 10^8 \ 1)$  and  
 550  $diag(10^6 \ 10^6 \ 9 \times 10^4)$ , respectively, while  $\mathbf{P}$  is the solution  
 551 of the discrete Algebraic Riccati equation. Whereas, for what  
 552 concerns the model initialization settings, they are resumed in  
 553 Table 5 and have been adopted for both testbed simulations  
 554 and experiments. Considering the computation time of the  
 555

557 TRMPC algorithm and sample time, we adopt a prediction  
 558 horizon of 20 in order to guarantee the stability of the sys-  
 559 tem and be compliant with the testbed constraint of maximum  
 560 computation time.

Table 5: FSS MPC design parameters and model initialization settings.

Parameter	Value
MPC Sample Time	3 [s]
Prediction Horizon	20
System Sample Time	0.01 [s]
GNC Sample Time	0.02 [s]
Maximum Simulation Time	450 [s]

561 According to the mission scenario described in the previous  
 562 Section, two different case studies have been selected, consid-  
 563 ering the following ICs:

- 564 1. Case A : (3.50 3.50 0 0 0 0), representing the optimal  
 565 case from a mission point of view, since the large margin  
 566 the Chaser has with respect to the cone boundaries,
- 567 2. Case B : (3.50 2.65 0 0 0 0), corresponding to the worst-  
 568 case scenario, where the spacecraft is close enough to one  
 569 of the cone limit that, in presence of uncertainty and  
 570 without a proper control, it could easily violate the cone  
 571 constraints.

572

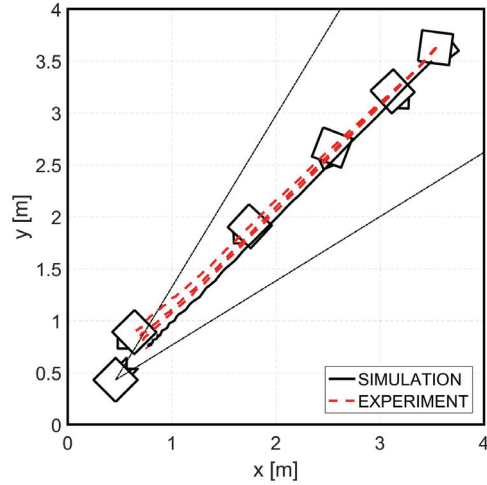
573 Each case study has been experimentally reproduced sev-  
 574 eral times, to validate the behavior of the controller. The result  
 575 analysis is based on the following performance parameters:

- 576 • Time-to-dock, which defines the total duration of the  
 577 maneuver performed by the Chaser to reach the Target,  
 578 starting from the initial condition;
- 579 • Control effort, which measures the efficiency of the con-  
 580 trol approach and represents a fuel consumption estima-  
 581 tion.

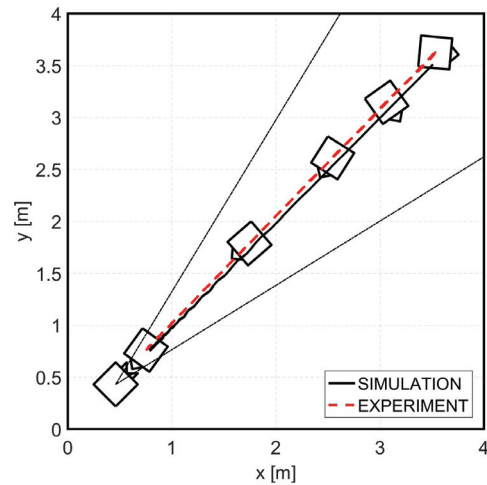
582 The controller performance in terms of computational time and  
 583 control effort are reported in Table 6 for Case A, and Tables  
 584 7 for Case B. In addition, the satisfaction or violation of the  
 585 constraints represents the third parameter in terms of how the  
 586 optimization-based controller is able to handle the disturbances  
 587 present in the system. Moreover, it is important to highlight  
 588 that all the trajectories depicted in Figures 6, 7 and 8 have  
 589 been obtained with respect to a minimum-effort performance  
 590 index. Indeed, while the rendezvous maneuver duration does  
 591 not represent a stringent constraint, the control effort is linked  
 592 to the fuel consumption as well as to the mission cost, hence it  
 593 shall be minimized.

## 594 7.2. Case A

595 The trajectories obtained in Case A are represented in Fig-  
 596 ure 6 for LQMPC and TRMPC, respectively. The first rele-  
 597 vant difference is related to the divergence of the experimental  
 598 trajectory with respect to the simulated one for the LQMPC  
 599 approach. This behavior can bring the Chaser to not dock  
 600 the Target at the end of the maneuver. In two over three  
 601 experiments, the Chaser missed the Target, for the LQMPC  
 602 approach, as shown in Figure 6(a). On the other hand, the  
 603 TRMPC approach shows a quasi-perfect match between the



(a) LQMPC



(b) TRMPC

Figure 6: Comparison of simulation and experimental trajectories in Case A. Three different experimental results are represented for each approach. The Chaser is represented at time  $t_0 = 0s$ ,  $t_1 = 20s$ ,  $t_2 = 100s$ ,  $t_3 = 200s$ .

604 simulation and experiment (see Figure 6(b), finalizing the tra-  
 605 jectory with the docking. In this case, even if the data reported  
 606 in Table 6 show that the robust approach is slower and more  
 607 fuel-consuming, i.e., the control effort is more than double in  
 608 the experimental environment, the main goal of the maneuver  
 609 is to bring the Chaser to dock the Target, even in presence  
 610 of persistent known disturbance. According to that, in this  
 611 case the LQMPC approach cannot satisfy this objective when  
 612 additive disturbance are acting on the system, since the drift  
 613 action brings the spacecraft far from the terminal position of  
 614 the Target.

Table 6: Performance of controllers in Case A (LQ=LQMPC, TR=TRMPC).

MPC Method	Time to-dock [s]	Control Effort [Ns]	Avg/Max Iter. [-]	Dock Y/N
LQ (sim.)	450.00	4.16	8.95/10	N
TR (sim.)	450.00	11.81	8.91/9	Y
LQ (exp.)	329.04	6.77	8.65/9	N
TR (exp.)	337.90	17.47	9.47/10	Y

615 7.3. Case B

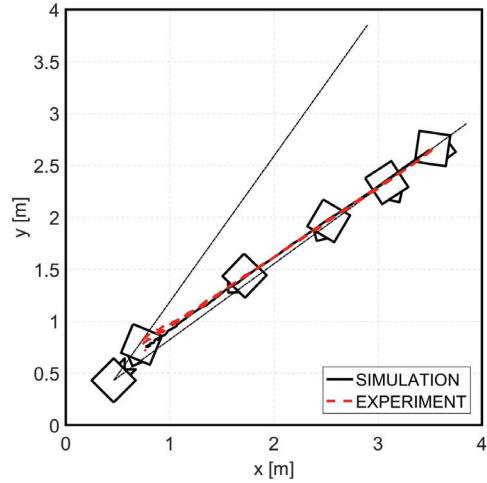
616 Case B represents the most critical one, because of the  
617 vicinity to the cone boundary. In this case, the docking condition  
618 is reached for both the approaches. However, there are several  
619 differences between the results obtained for the two MPC  
620 methods, as represented in Figure 7 and according to the controllers  
621 performance parameters in Tables 6 and 7. In the second scenario,  
622 the LQMPC also allows a faster maneuver, even if the difference is  
623 significant only comparing the experimental results. Considering the  
624 control effort, the TRMPC proves itself to be the more fuel consuming  
625 approach, in the order of two/three times more. Nonetheless, in terms  
626 of constraint satisfaction, the robust approach validates its robustness  
627 to bounded additive disturbance (see Figure 7(b)), whereas the  
628 classical approach cannot deal with the uncertainty properly, as  
629 shown in Figure 7(a), specially in the last part of the maneuver,  
630 as highlighted in Figure 8. In fact, in the latter case, the Chaser  
631 violates the cone boundary, failing the docking in the experimental  
632 set up (see Figure 8(a)) and the required attitude is not well-achieved.  
634

Table 7: Performance of controllers in Case B (LQ=LQMPC, TR=TRMPC).

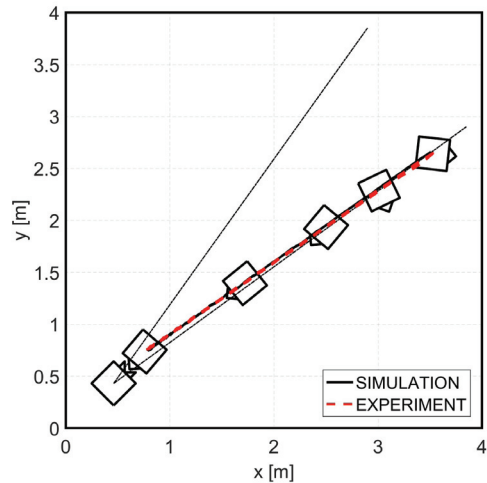
MPC Method	Time to-dock [s]	Control Effort [Ns]	Avg/Max Iter. [-]	Dock Y/N
LQ (sim.)	450.00	3.82	8.94/10	Y
TR (sim.)	450.00	11.60	8.90/9	Y
LQ (exp.)	301.13	5.22	8.58/9	Y
TR (exp.)	320.65	16.07	9.46/10	Y

635 8. Conclusions

636 Considering the maneuver of rendezvous and docking (RVD)  
637 between two spacecraft as a mission scenario, the performance  
638 of two Model Predictive Control (MPC) schemes, one deterministic  
639 and one robust, have been compared in presence of persistent  
640 additive disturbance. A Tube-based Robust MPC (TRMPC),  
641 related to the approach already proposed in literature,  
642 has been adopted for the first time within this scenario as  
643 robust scheme, to guarantee robustness and suitable computational  
644 effort for real-time implementations. The stability of this  
645 robust scheme is ensured through a Linear Matrix Inequalities  
646 (LMI) approach, taking into account possible parametric  
647 uncertainty representing unmodelled dynamics, and neglected  
648 nonlinearities. Focusing on the robust approach, the Chaser  
649 spacecraft satisfies the hard state and control constraints and  
650 performs an autonomous docking with the Target, both in  
651 simulation (three degree-of-freedom (DoF) orbital simulator) and  
652 experimental environment (three DoF air-bearing testbed). On



(a) LQMPC

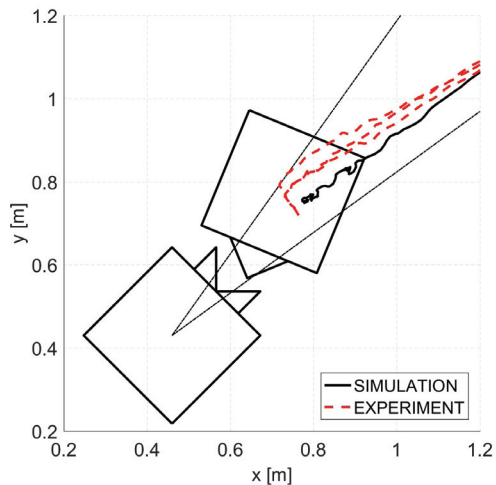


(b) TRMPC

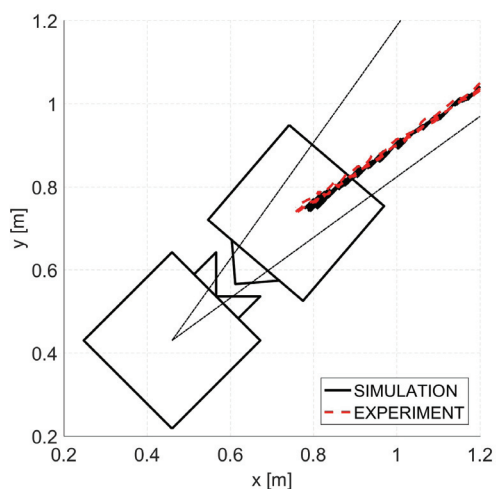
Figure 7: Comparison of simulation and experimental trajectories in Case B. Three different experimental results are represented for each approach. The Chaser is represented at time  $t_0 = 0s$ ,  $t_1 = 20s$ ,  $t_2 = 100s$ ,  $t_3 = 200s$ .

653 the other hand, the deterministic LQMPC is not always able to  
654 satisfy the state and input constraints, especially, in terms of  
655 cone boundaries, i.e., the Chaser cannot dock the Target. The  
656 results shown that they can be implemented on-board for the  
657 real-time control of the final phase of the RVD maneuver, with  
658 a comparable computational effort, even if the fuel consumption  
659 is higher when the robust approach is adopted. Hence, if  
660 the constraint satisfaction represents the main mission requirement,  
661 the TRMPC guarantees better performance.

662 In this work, -V-bar approach has been chosen as capture  
663 axis, referring to the RVD mission profile of Soyuz, Progress



(a) LQMPC



(b) TRMPC

Figure 8: Zoomed-in trajectory of Case B for LQMPC and TRMPC. Three different experimental results are represented for each approach.

664 and ATV vehicles. The effectiveness of the controller is ensured  
 665 by the terminal cost, defined with respect to the reference final position  
 666 to be reached and the control strategy is not tailored with respect to the  
 667 scenario considered, from a theoretical viewpoint. Finally, a tracking  
 668 approach could be exploited, driving the error between the actual state  
 669 and the desired one to zero. In this case, the TRMPC approach also  
 670 remains valid and all the properties stand if the cost function as well as  
 671 the state constraint set are re-defined with respect to the deviation  
 672  $\delta x = x - x_{ref}$ . Thanks to the flexibility of the proposed controller,  
 673 it could be exploited also for different space scenarios  
 674

675 such as: (a) R-bar approach, considering the mission profile  
 676 of Soyuz and Progress vehicles on the nadir pointing side of  
 677 the ISS Docking and Storage Module; (b) station-keeping; (c)  
 678 attitude control, accounting for various mission objectives and  
 679 type of spacecraft.

## Acknowledgments

680 The authors wish to thank Roberto Tempo and Fabrizio  
 681 Dabbene, at CNR-IEIIT, Politecnico di Torino, and Matthias  
 682 Lorentzen, at Institute for Systems Theory and Automatic Control  
 683 of the University of Stuttgart, for their precious support  
 684 provided for the theoretical definition of the TRMPC problem.  
 685 The authors would also thank Josep Virgili-Llop and Costantino  
 686 Zagaris, at the Naval Postgraduate School, for the support  
 687 in performing experiments.  
 688

## References

- 689
- [1] Subbarao, K., and Welsh, S., "Nonlinear Control of Motion Synchronization for Satellite Proximity Operations," *Journal of Guidance, Control, and Dynamics*, vol. 31(5), pp. 1284-1294, 2008.
  - [2] Lee, D., Cochran, J., Jr., and No, T., "Robust Position and Attitude Control for Spacecraft Formation Flying", *Journal of Aerospace Engineering*, vol. 25 (3), pp. 436-447, 2012.
  - [3] Capello, E., Punta, E., Dabbene, F., Guglieri, G., and Tempo, R., "Sliding Mode Control Strategies for Rendezvous and Docking Maneuvers", *Journal of Guidance, Dynamics and Control*, vol. 40 (6), pp. 1481-1487, 2017.
  - [4] Luo, Y., Zhang, J., and Tang, G., "Survey of Orbital Dynamics and Control of Space Rendezvous", *Chinese Journal of Aeronautics*, vol. 27 (1), pp. 1-11, 2014.
  - [5] Rybus, T., and Seweryn, K., "Planar Air-bearing Microgravity Simulators: Review of Applications, Existing Solutions and Design Parameters", *Acta Astronautica*, vol. 120, pp. 239-259, 2016.
  - [6] Di Cairano, S., Park, H., and Kolmanovsky, I., "Model Predictive Control Approach for Guidance of Spacecraft Rendezvous and Proximity Maneuvering", *International Journal of Robust and Nonlinear Control*, vol. 22 (12), pp. 1398-1427, 2012.
  - [7] Leomanni, M., Rogers, E., and Gabriel, S. B., "Explicit Model Predictive Control Approach for Low-Thrust Spacecraft Proximity Operations", *Journal of Guidance, Control, and Dynamics*, vol. 37(6), pp. 1780-1790, 2014.
  - [8] Gavilan, F., Vazquez, R., and Camacho, E. F., "Robust Model Predictive Control for Spacecraft Rendezvous with Online Prediction of Disturbance Bounds", 2011.
  - [9] B. Kouvaritakis, B., and Cannon, M., "Model Predictive Control: Classical, Robust and Stochastic", *Advanced Textbooks in Control and Signal Processing*, Springer, 2015.
  - [10] Graichen, K., and Kapernick, B., "A Real-Time Gradient Method for Nonlinear Model Predictive Control", "Frontiers of Model Predictive Control", book edited by Tao Zheng, 2012.
  - [11] Mayne, D. Q., Rawlings, J. B., "Model Predictive Control: Theory and Design", *Madison, WI: Nob Hill Publishing, LCC*, 2009.
  - [12] Granado, E., Colmenares, W., Bernussou, J., and Garcia, G., "Linear matrix inequality based model predictive controller", *IEEE Proceedings Control Theory and Applications*, vol. 50 (5), 2003.
  - [13] Fu, Y., and Li, C., "Parametric method for spacecraft trajectory tracking control problem with stochastic thruster fault", *IET Control Theory and Applications*, vol. 10 (17), pp. 2331-2338, 2016.
  - [14] Clohessy, W. H., Wiltshire, R. S., "Terminal Guidance System for Satellite Rendezvous", *Journal of the Aerospace Sciences*, Vol. 27 (9), pp. 653-658, 1960.
- 720  
721  
722  
723  
724  
725  
726  
727  
728  
729  
730  
731  
732  
733  
734  
735  
736  
737  
738

- 739 [15] Virgili-Llop, J., Zagaris, C., Park, H., Zappulla II, R., and Romano, M., "Experimental evaluation of model predictive control and inverse dynamics control for spacecraft proximity and docking maneuvers", *CEAS Space Journal*, vol. 10(1), pp 37–49, 2018.
- 744 [16] Barmish, B. R., "New Tools for Robustness of Linear Systems", *Macmillan Publishing Company*, New York, 1994.
- 746 [17] Zappulla II, R., Virgili-Llop, J., Zagaris, C., Park, H., and Romano, M., "Dynamic Air-Bearing Hardware-in-the-Loop Testbed to Experimentally Evaluate Autonomous Spacecraft Proximity Maneuvers", *Journal of Spacecraft and Rockets*, 2017.
- 751 [18] Fehse, W., "Automated Rendezvous and Docking of Spacecraft", *Cambridge University Press*, vol. 16, 2003.
- 753 [19] Dentis, M., Capello, E., Guglieri, G., "A Novel Concept for Guidance and Control of Spacecraft Orbital Maneuvers", *International Journal of Aerospace Engineering*, vol. 2016, Article ID 7695257, 14 pages, 2016. doi:10.1155/2016/7695257.
- 757 [20] Lugini, C., and Romano, M., "A Ballistic-Pendulum Test Stand to Characterize Small Cold-gas Thruster Nozzles.", *Acta Astronautica*, vol. 64, pp. 615-625, 2009.
- 760 [21] Bartlett, A. C., Hollot, C. V., Huang, L., "Root Locations of an Entire Polytope of Polynomials: It Suffices to Check the Edges", *Mathematics of Control, Signals, and Systems*, vol.1, pp. 61-71, 1988.
- 764 [22] Tempo, R., Calafiore, G., and Dabbene, F., "Randomized Algorithms for Analysis and Control Uncertain Systems", *Springer Science & Business Media*, 2012.
- 767 [23] Chisci, L., Rossiter, J. A., and Zappa, G., "Systems with Persistent Disturbances: Predictive Control with Restricted Constraints", *Automatica*, vol. 37 (7), pp. 1019-1028, 2001.
- 770 [24] Lorenzen, M., Dabbene, F., Tempo, R., and Allgöwer, F., "Constraint-Tightening and Stability in Stochastic Model Predictive Control", *IEEE Transactions on Automatic Control*, 2016.
- 774 [25] Rakovic, S. V., Kerrigan, E. C., Kouramas, K., and Mayne, D. Q., "Approximation of the Minimal Robustly Positively Invariant Set for Discrete-time LTI Systems with Persistent State Disturbances", *42nd IEEE Conference on Decision and Control*, Maui, Hawaii, 2003.
- 779 [26] Saponara, M., Barrena, V., Bemporad, A., Hartley, E. N., Maciejowski, J., Richards, A., Tramutola, A., and Trodden, P., "Model Predictive Control Application to Spacecraft Rendezvous in Mars Sample & Return Scenario", *Proceeding of 4th European Conference for Aerospace Sciences*, Saint Petersburg, Russia, 2011.
- 785 [27] Bodin, P., Noteborn, R., Larsson, R., and Chasset, C., "System Test Results from the GNC Experiments on the PRISMA in-orbit Test Bed", *Acta Astronautica*, vol. 68 (7), pp. 862-872, 2011.
- 789 [28] Zappulla R., Virgili-Llop J., and Romano M., "Spacecraft Thruster Control via Sigma-Delta Modulation". *Journal of Guidance, Control, and Dynamics*. Accepted for Publication, vol. 40 (11), pp. 2928-2933, 2017.